Preprints (www.preprints.org) | NOT PEER-REVIEWED | Posted: 27 January 2022 doi:10.20944/preprints202201.0409.v1

Nonlinear investigation of Gol'denveizer's problem of a circular and elliptic elastic torus

Guang-Kai Song[1] and Bo-Hua Sun[1,*]

[1]School of Civil Engineering & Institute of Mechanics and Technology, Xi'an University of Architecture and Technology, Xi'an 710055, China.

Gol'denveizer's problem of a torus has been analyzed by Audoly and Pomeau (2002) and Sun (2021). However, all of the investigations of Gol'denveizer's problem of an elastic torus have been linear. In this paper, the finite element method is used to more accurately address this problem. Furthermore, Sun (2021) cannot be solved by nonlinear analysis. We research the nonlinear mechanical properties of Gol'denveizer's problem of circular and elliptic tori, and relevant nephograms are given. We study the buckling of Gol'denveizer's problem of an elastic torus, and propose failure patterns and force-displacement curves of tori in the nonlinear range. Investigations reveal that circular tori have more rich buckling phenomena as the parameter a increases. Gol'denveizer's problem of the buckling of an elliptic torus is analyzed, and we find a new buckling phenomenon called a "skirt." As a/b increases, the collapse load of an elliptic torus of the Gol'denveizer problem is enhanced gradually.

I. INTRODUCTION

The shell structure is widely used in engineering and aviation. It is important to note the superior mechanical properties of the toroidal shell, as compared to the complicated topology of the torus. The culprit is Gaussian curvature, $K = \frac{\sin\theta}{a(R+a\sin\theta)}$. The major radius of curvature K changes with θ,

$$K = \frac{\sin\theta}{a(R+a\sin\theta)} = \begin{cases} <0, & \theta \in [-\pi, 0] \\ =0, & \theta = 0 \\ >0, & \theta \in [0, \pi]. \end{cases} \tag{1}$$

The geometry of a torus is shown in Figure 1.

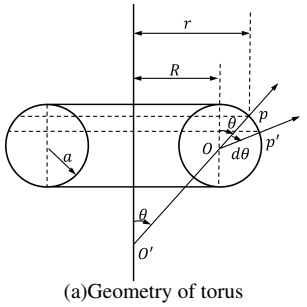

(a)Geometry of torus

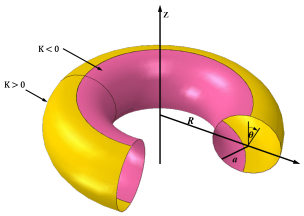

(b)Gaussian curvature partition and cross-section

Figure 1: Geometric characteristics of torus. Radii of curvature are $R_1 = a, R_2 = \frac{R+a\sin\theta}{\sin\theta}$; major curvatures are $K_1 = \frac{1}{R_1}, K_2 = \frac{1}{R_2}$; Gaussian curvature $K = K_1K_2 = \frac{\sin\theta}{a(R+a\sin\theta)}$.

Many researchers have investigated the mechanics of a toroidal shell. Early work examined the stress and mechanical properties of elastic tori of mixed types [1]-[9]. Sun[10] proposed a new real-form ODE system and implied that the deformation and stress response of an elastic torus are sensitive to the radius ratio, and Sun [11]demonstrated that the nonlinear deformation analysis of a Mindlin torus can be replaced by a simple equation.

The Gol'denveizer problem is well known: a toroidal shell is loaded under axial forces and the outer and inner equators are loaded with opposite balanced forces. Gol'denveizer [12] proposed that the membrane theory of shells does not yield a valid solution in this situation. Flügge [13] proposed the same problem for an oblique elliptic torus, and this was settled by Sun [14]. Audoly and Pomeau [15]-[16]studied the Gol'denveizer problem, and they proved that Gol'denveizer's conclusion is correct. They made use of a membrane solution of a toroidal shell and nonlinear boundary-layer perturbation to obtain an approximate solution of torus deformation around the crown, and they gave a simple formula relating force F and vertical displacement,

$$F = \frac{4Eh^2}{a\sqrt{12(1-\mu^2)}}\Delta_z, \tag{2}$$

where E and μ are the elastic modulus and Poisson's ratio, respectively, of the torus, and other parameters are shown in Figure 2.

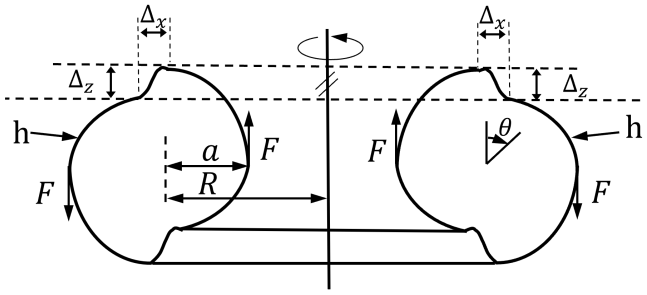

Figure 2: Cross-section of deformed torus.

Sun [17] used the bending theory of shells to solve the Gol'denveizer problem, showed that the membrane theory of a torus leads to a singular solution, proved that the solution of Audoly and Pomeau [15]-[16] had a certain accuracy, and proposed that the bending theory of shells should be used to unravel the Gol'denveizer problem.

*Corresponding author:sunbohua@xauat.edu.cn

Preprints (www.preprints.org) | NOT PEER-REVIEWED | Posted: 27 January 2022 doi:10.20944/preprints202201.0409.v1

The results of Audoly and Pomeau [15]-[16] and Sun [17] are in the linear range of a circular torus. We conduct a nonlinear investigation of the Gol'denveizer problem of a circular or elliptic torus, which, to the best of our knowledge, has not been addressed in the literature.

The remainder of this paper is organized as follows. Section 2 presents the finite element model and ABAQUS settings, and finite element results are compared with the theoretical solutions of Sun [17] and Audoly [15]. Section 3 discusses the finite element analysis of the nonlinear behavior of elliptic and circular tori, such as bending moment, membrane force, shear force, and displacement. Section 4 presents the buckling analysis of circular and elliptic tori of the Gol'denveizer problem using FE analysis. Section 5 presents conclusions and perspectives.

II. FINITE ELEMENT MODELING AND VERIFICATION

A. Finite element modeling of a circular torus

We apply the finite element method (FEM) to the Gol'denveizer problem of a circular torus, and based on the data in Table 1, the radius changes ($a = 0.3k, k = 1, 2, 3$), but the other quantities remain constant. For efficient calculation, we choose the half-circular torus in ABAQUS, as simulated by three-dimensional (3D) deformable bodies, considering the shell edge load. The outer and inner equators are loaded with opposite balanced forces $F = 1N$. A number of mesh types are provided in ABAQUS, but many their elements have poor suitability and cause non-convergence of the solution. We use reduced integration linear shell elements (S4R) for their accuracy, reliability, and speed, where the mesh size is $2mm$. The details of the FE model are shown in Table 1 and Figure 3.

Table I: Data of circular torus in FEM.

Quantity[1]	a	R	h	ρ	E	μ	F
Unit	m	m	m	kg/m^3	N/m^2	1	N
Data	$0.3k$	1	0.05	7800	2.07×10^{11}	0.3	1

[1]Figure 1 shows a, R. Parameters h, ρ, E, μ are thickness, density, elastic modulus, and Poisson's ratio, respectively.

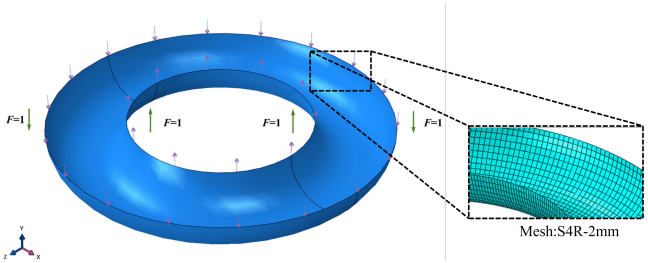

Figure 3: Details of FEM model with shell edge load and force $1N$. Mesh has 4-node reduced integration shell elements (S4R), and mesh size is $2mm$.

We calculate the theoretical solution of a half-circular torus ($\theta \in [\pi/2, 3\pi/2]$) of Sun [17], and we compare this to our FE results to verify our method.

B. Verification of finite element method

We validate the FEM by comparison with the vertical displacement results of Sun [17]. Table 2 presents the results of Audoly and Pomeau [15], based on membrane theory and boundary layer analysis, our finding by the use of FEM, and the results of Sun [17] based on the full bending theory of a half-circular torus. Our result agrees well with the data, demonstrating the usefulness of finite element methods to solve Gol'denveizer's problem of an elastic torus. Moreover, it will be seen that the three methods have the same results. It is inconceivable that the outcome of Audoly and Pomeau[15] is a good prediction. The results of Sun [17] are more accurate; hence, bending theory, which uses the major radius R, is suitable for investigating the mechanics of the problem, and in the theory of Audoly and Pomeau [15], R is omitted.

Table II: Vertical deformation $\Delta_z[m]$.

	$\Delta_z(a = 0.3)$	$\Delta_z(a = 0.6)$	$\Delta_z(a = 0.9)$
Finite element analysis	$4.2798e-10$	$0.9844e-9$	$1.4666e-9$
Sun [17]	$4.3219e-10$	$0.9677e-9$	$1.4484e-9$
Audoly and Pomeau [15]	$4.7892e-10$	$0.9578e-9$	$1.4368e-9$

The bending theory of Sun [17] and the theory of Audoly and Pomeau [15], both based on dimensional and boundary layer analysis, can explain the Gol'denveizer problem of a torus, and the final result of bending theory is more accurate than that of Audoly and Pomeau; these two theories also prove that our FEMs can solve the Gol'denveizer problem of the torus.

III. NONLINEAR MECHANICAL PROPERTY ANALYSIS OF GOL'DENVEIZER PROBLEM

We can see that the investigation of Sun [17] is linear. There is limited nonlinear study of this problem, and no one knows the nonlinear mechanics of Gol'denveizer's problem of elliptic tori and toroidal shells. We will use FEMs to research the nonlinear mechanics of the Gol'denveizer problem of circular and elliptic tori. FEMS are good for nonlinear analysis, and the FE analysis program ABAQUS has many nonlinear means to study large deformations. We use a quasi-static step and S4R mesh to investigate the nonlinear Gol'denveizer problem of three circular torus models with radii $a = 0.3k, k = 1, 2, 3$, and force $F = 1 \times 10^8 N$, and an elliptic torus with parameter $a/b = 2, 3, 4$, and force $F = 3 \times 10^7 N$. Incidentally, the research of Sun [14] gave the principle radii of the oblique elliptic torus as

$$r_1 = \frac{a^2 b^2}{(a^2 \sin^2\theta + b^2 \cos^2\theta)^{3/2}}, \tag{3}$$

Preprints (www.preprints.org) | NOT PEER-REVIEWED | Posted: 27 January 2022 doi:10.20944/preprints202201.0409.v1

$$r_2 = \frac{1}{\sin(\theta+\beta)}\left[R + \frac{a^2\sin\theta\cos\beta + b^2\cos\theta\sin\beta}{(a^2\sin^2\theta + b^2\cos^2\theta)^{1/2}}\right], \tag{4}$$

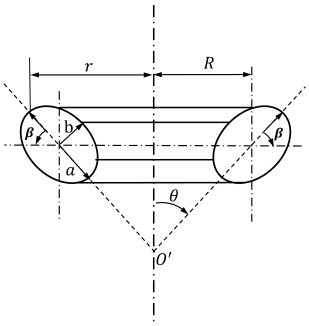

Figure 4: Geometry of oblique elliptic torus.

where β is an oblique angle, and other parameters are shown in Figure 4. The geometric characteristics of elliptic and circular tori are shown in Figure 5. Other parameters of the model are shown in Tables 1 and 3.

Table III: Data of half-elliptic torus in FEM.

Quantity[1]	a	b	R	h	ρ	E	μ	F
Units	m	m	m	m	kg/m^3	N/m^2	1	N
Data 1	0.3	0.15	1	0.05	7800	2.07×10^{11}	0.3	3×10^7
Data 2	0.3	0.1	1	0.05	7800	2.07×10^{11}	0.3	3×10^7
Data 3	0.3	0.075	1	0.05	7800	2.07×10^{11}	0.3	3×10^7

[1]Radii a, b, R are shown in Figure 3(c). Parameters h, ρ, E, μ are thickness, density, elastic modulus, and Poisson's ratio of an elliptic torus, respectively. $a/b = 2, 3, 4$.

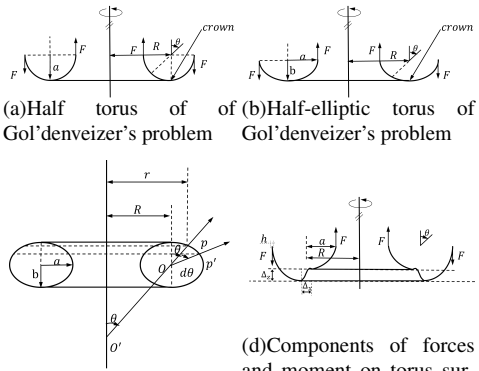

(a)Half torus of Gol'denveizer's problem

(b)Half-elliptic torus of Gol'denveizer's problem

(c)Geometry of elliptic torus

(d)Components of forces and moment on torus surface

Figure 5: Geometric characteristics of elliptic and circular tori. When $a = b$, the elliptic torus becomes a circular torus with radius a. In the elliptic torus, a and b present the major and minor axes, respectively.

A. Deformation analysis

The nonlinear analyses of the horizontal displacement of half-circular and half-elliptic tori are shown in Figures 6 and 7, respectively. The corresponding vertical displacements are analyzed in Figures 8 and 9, respectively. As we shall see, the maximum negative horizontal displacement does not occur to the crowns at $\theta = \pi$ of a half-circular torus. With $\theta = \pi/2$, the horizontal displacement decreases as the radius a increases. For vertical displacements, the curve has some of the same tendencies as it does in the linear study. However, for a half-circular torus, various values of vertical displacements are shown in a nonlinear study when the $\theta = \pi/2$, and the values cannot be close to zero. This conflicts with the linear results.

The vertical displacements of a half-elliptic torus gradually increase with the parameter a/b. Compared to a circular torus, the vertical displacement curves of the half-elliptic torus do not exhibit displacement platform phenomena. Moreover, the three vertical displacement curves do not intersect. Figure 7 shows the horizontal displacements of a half-elliptic torus. It can be seen that the three curves have the same trend, and as a/b increases, the horizontal displacements decrease and gradually diverge from the crown line. When $\theta = \pi/2$, the horizontal displacements decrease as a/b increases.

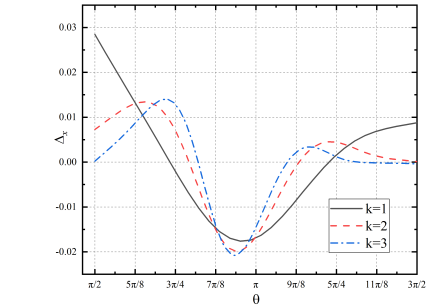

(a)Horizontal displacement of half-circular torus

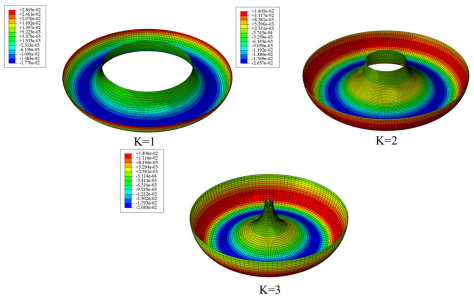

(b)Horizontal displacement nephograms of half-circular torus

Figure 6: Horizontal displacement of circular torus: radius $a = 0.3k, k = 1, 2, 3$. For nephograms of half-circular torus, colors represent different horizontal displacements. Δ_x has unit $[m]$.

Preprints (www.preprints.org) | NOT PEER-REVIEWED | Posted: 27 January 2022 doi:10.20944/preprints202201.0409.v1

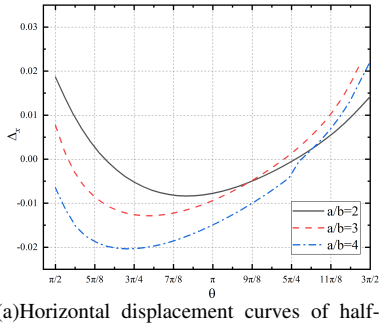

(a)Horizontal displacement curves of half-elliptic torus

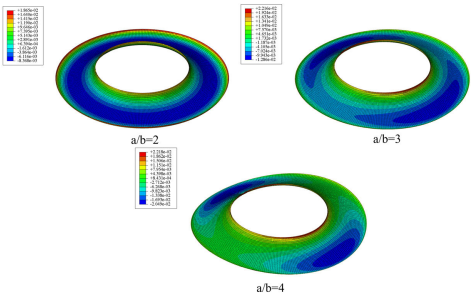

(b)Horizontal displacement nephograms of half-elliptic torus

Figure 7: Horizontal displacement of elliptic torus: a and b present major and minor axes, respectively. When $a = b$, the elliptic torus becomes a circular torus with radius a. For nephograms of a half-elliptic torus, as a/b increases, the blue area gradually decreases. Δ_x has unit $[m]$.

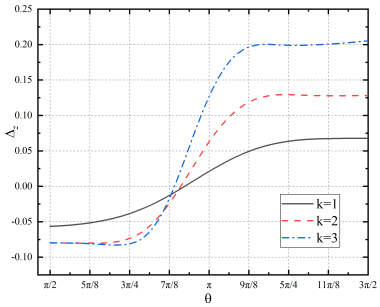

(a)Vertical displacement curves of half-circular torus

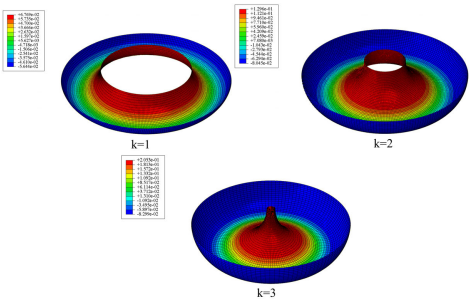

(b)Vertical displacement nephograms of half-circular torus

Figure 8: Vertical displacement of circular torus: radius $a = 0.3k, k = 1, 2, 3$; Δ_z has unit $[m]$.

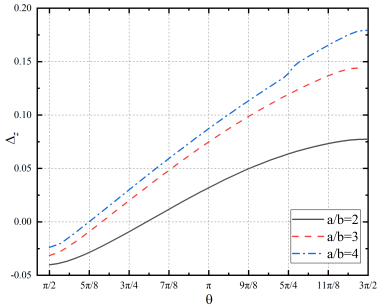

(a)Vertical displacement curves of half-elliptic torus

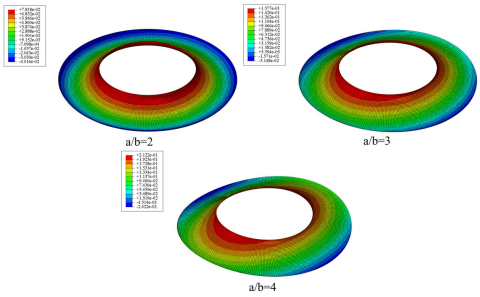

(b)Vertical displacement nephograms of half-elliptic torus

Figure 9: Vertical displacement of elliptic torus: a and b present major and minor axes, respectively. When $a = b$, the elliptic torus become circular, with radius a. For nephograms of half-elliptic torus, red area for elliptic torus changes from circle to ellipse. Δ_z has unit $[m]$.

To investigate the nonlinear deformation of the Gol'denveizer problem, we display nephograms of horizontal and vertical displacements in Figures 6 and 8, from which we find that the torus undergoes obvious deformation. The displacement distribution is triaxial symmetry, and colors of nephograms represent changes of displacement. We note that the horizontal displacement of a circular torus changes greatly as k increases. Notably, for the horizontal and vertical displacement nephograms of an elliptic torus, the colors are distributed nonuniformly. This means that elliptic tori appear to have an asymmetric deformation when $F = 3 \times 10^7 N$, and the horizontal displacements on the same latitude line are unequal. Vertical displacements follow the same rule.

B. Bending moment, membrane force, and shear force analysis

Figures 10–15 show the bending moment, membrane force, and shear force calculated using the nonlinear finite element method, from which we see much difference on the crown line ($\theta = \pi$) of the half-circular torus. The bending moments of three models ($k = 1, 2, 3$) are equal at the crown ($\theta = \pi$) by linear calculation, but in the nonlinear analysis, for the bending moment, the crown line is no longer unique, and the point where $M_1 = 0$ can be found at $\theta = 7\pi/8$ and not on the crown line ($\theta = \pi$). The same phenomenon occurs for the membrane and shear force. As k decreases, the maximum shear force is closer to the crown line. For an elliptic torus,

Preprints (www.preprints.org) | NOT PEER-REVIEWED | Posted: 27 January 2022 doi:10.20944/preprints202201.0409.v1

when $\theta = \pi$, a plateau for the force-θ curves occurs because the curvature in the crown line decreases when b is less than a.

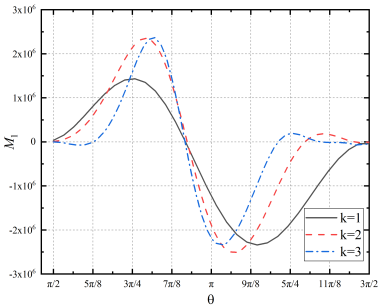

(a)Bending moment curves of half-circular torus

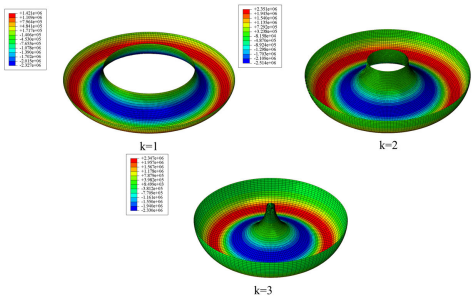

(b)Bending moment nephograms of half-circular torus

Figure 10: Bending moment M_1 of half-circular torus: radius of circular torus $a = 0.3k, k = 1, 2, 3$; colors represent different bending moments of half-circular torus. M_1 has units $[N \cdot m]$.

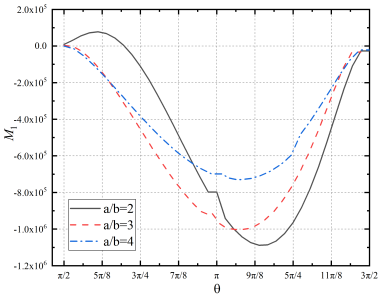

(a)Bending moment curves of half-elliptic torus

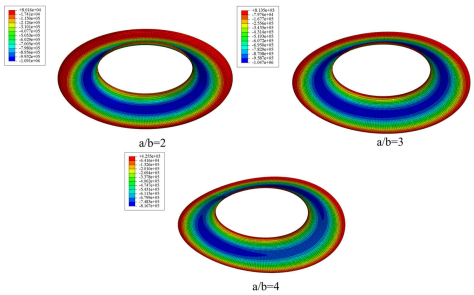

(b)Bending moment nephograms of half-elliptic torus

Figure 11: Bending moment M_1 of half-elliptic torus: a and b present major and minor axes, respectively. As a/b increases, the bending moment of the elliptic torus decreases. M_1 has units $[N \cdot m]$.

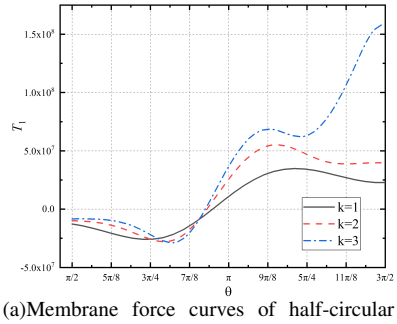

(a)Membrane force curves of half-circular torus

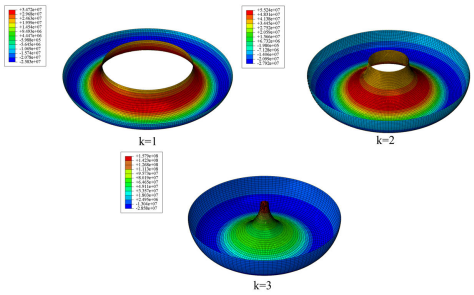

(b)Membrane force nephograms of half-circular torus

Figure 12: Membrane force T_1 of half-circular torus: radius $a = 0.3k, k = 1, 2, 3$; colors represent different bending moments. T_1 has unit $[N]$.

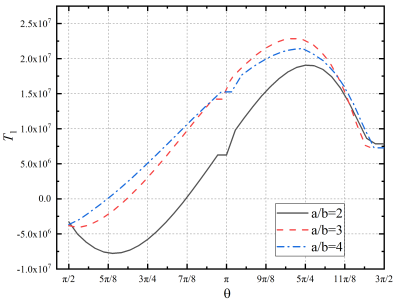

(a)Membrane force curves of half-elliptic torus

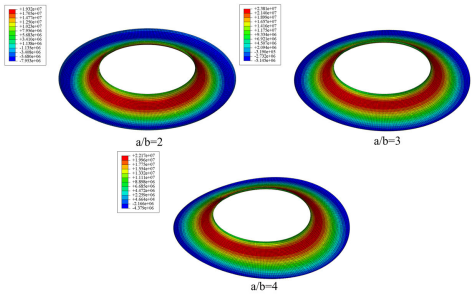

(b)Membrane force nephograms of half-elliptic torus

Figure 13: Membrane force T_1 of half-elliptic torus: a and b present major and minor axes, respectively. When $a = b$, the elliptic torus becomes a circular torus with radius a. Colors represent different bending moments. T_1 has unit $[N]$.

Preprints (www.preprints.org) | NOT PEER-REVIEWED | Posted: 27 January 2022 doi:10.20944/preprints202201.0409.v1

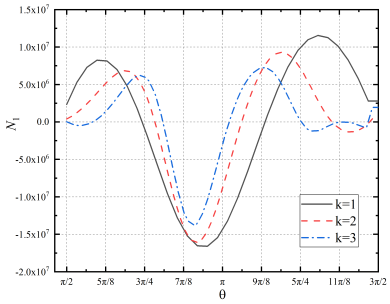

(a)Shear force curves of half-circular torus

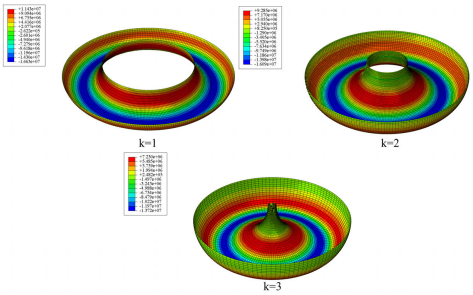

(b)Shear force nephograms of half-circular torus

Figure 14: Shear force N_1 of half-circular torus: radius of circular torus $a = 0.3k, k = 1, 2, 3$; For shear force curves, the value of minor force decreases gradually as k increases. For shear force nephogram, colors represent different shear force. N_1 has unit $[N]$.

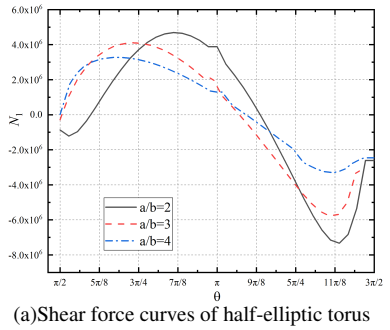

(a)Shear force curves of half-elliptic torus

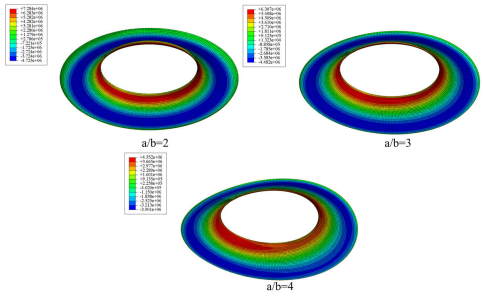

(b)Shear force nephograms of half-elliptic torus

Figure 15: Shear force N_1 of half-elliptic torus: as a/b increases, the peak value of shear force decreases gradually. In elliptic torus, a and b present major and minor axes, respectively. For shear force nephogram, colors represent different shear force. N_1 has unit $[N]$.

We also provide a nephogram of the bending moment, membrane force, and shear force for an elliptic torus and toroidal shell, where forces are represented by different colors, so as to represent the nonlinear mechanism of the Gol'denveizer problem as simply as possible. For instance, the red part indicates maximum force under a negative Gaussian distribution. We remark that the negative Gaussian part of a circular torus has a stronger bearing than the positive Gaussian part. The force nephograms of a circular and elliptic torus show the same force at the same latitude line.

C. Elastic energy density

The Figures 16 show the energy density nephograms of half circular and elliptic torus. The total elastic energy density are represented by different colors in this nephograms. The red part indicates maximum felastic energy density of half circular and elliptic torus. For the half circular torus, the red part appears in the negative Gaussian curvature part near the crown line, it's means that the bearing capacity of negative Gaussian curvature is higher than positive Gaussian curvature in half circular torus. For half elliptic torus, with the a/b increases, the area of light blue gradually decreases, the elliptic tori appear to have an asymmetric deformation. So the energy density nephograms can help us to investigate Gol'denveizer's Problem of a circular or elliptic elastic torus clearly.

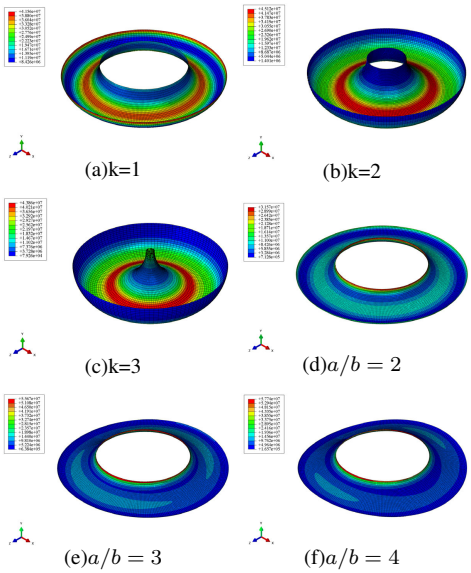

(a)k=1 (b)k=2 (c)k=3 (d)$a/b = 2$ (e)$a/b = 3$ (f)$a/b = 4$

Figure 16: Elastic energy density nephograms of half circular and elliptic torus

IV. BUCKLING ANALYSIS OF GOL'DENVEIZER PROBLEM

A. Buckling phenomenon of Gol'denveizer problem of circular torus

Above, we found the nonlinear mechanism of the Gol'denveizer problem and plotted curves of force and dis-

Preprints (www.preprints.org) | NOT PEER-REVIEWED | Posted: 27 January 2022 doi:10.20944/preprints202201.0409.v1

placement versus θ, but we did not obtain the failure patterns of elastic toroidal shells. Hence, we use the finite element method to investigate the buckling of elastic circular and elliptic tori whose outer and inner equators are loaded with opposite balanced forces. For convenience in finding the buckling phenomena of circular and elliptic tori, we replace balanced forces with balanced displacement. The model has $a = 0.3, 0.6, 0.9$ for a half-circular torus, with the same FEM parameters as above. The curves of force versus displacement are shown in Figure 17.

We find that the buckling of a half-circular torus shows different phenomena as a changes. A model with smaller a has a smooth curve and similar buckling failure. When $a = 0.3$, the inner and outer equator of the torus show interlaced deformation. A half-circular torus becomes round at a displacement of $0.25m$. Failure modes vary as a increases. Figure 17(b) shows the new phenomena of indentations and intumescentia of the shell. Before peak points of curves, the deformation is axisymmetric, but when we pass through a peak, there is much change. The deformation of a half-circular torus is wave-like and nonaxisymmetric. As the displacement increases, the four vertices of indentations become two, the intumescentia of shells take the shape of a long ridge, and inner equators become elliptic. In Figure 17(c), the model with $a = 0.9m$ has more rich buckling phenomena. After the four vertices of indentation occur, the number of intumescentia of a half-circular torus does not change, but the damage degree grows with the displacement. Asymmetric failure of a half-circular torus occurs in the later stage of loading.

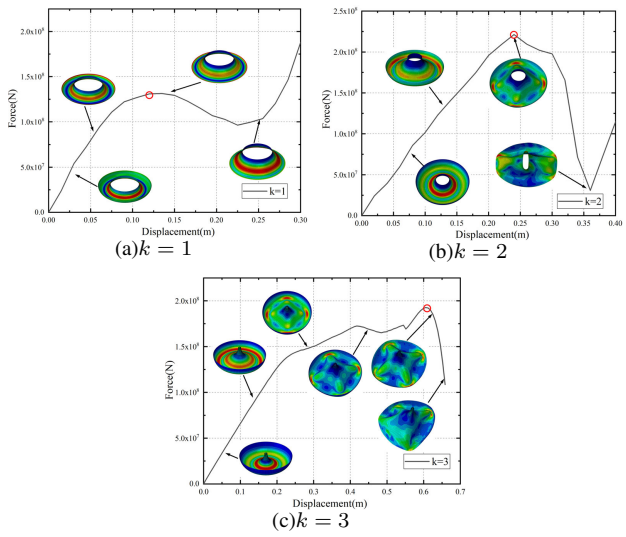

(a)$k = 1$ (b)$k = 2$

(c)$k = 3$

Figure 17: Force-versus-displacement curves for FEM specimens with a radius $a = 0.3k[m]$. The deformation diagram represents failure modes of structures in different periods. Red circle indicates collapse load of circular torus.

B. Buckling analysis of Gol'denveizer problem of elliptic torus

To obtain failure patterns of the Gol'denveizer problem of an elliptic toroidal shell, we use ABAQUS to simulate a half-elliptic torus with $a/b = 2, 3, 4$, whose data are shown in Table 3, and whose curves of force versus displacement and failure patterns are shown in Figure 18.

The simulations show some buckling manifestation. When the minor displacement of equators occurs, the deformation is not obvious. When the displacement increases, the inner equator of a half-elliptic torus decreases and the outer equator increases, and the shape of the torus turns into a round platform. We call this a "skirt" shape. A wrinkle then appears in the bottom part, which gradually becomes more apparent with displacement. For wrinkles in the bottom part of the half-elliptic torus, it is just like the swing of a skirt. To this point, different axisymmetric deformation patterns have occurred. However, at the peak of the force-versus-displacement curves, they drop sharply and the deformation becomes skewed. Serious buckling occurs, and the peak of the curve is the collapsed point of the Gol'denveizer problem.

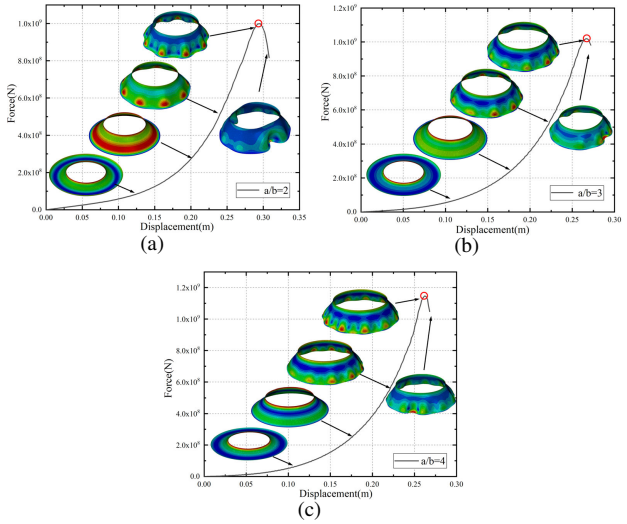

(a) (b)

(c)

Figure 18: Force-versus-displacement curves for specimens: (a) $a/b = 2$; (b) $a/b = 3$; (c) $a/b = 4$. Parameters a and b are major and minor axes, respectively, of elliptic torus. Deformation diagram represents failure modes of structures in different periods. Red circle indicates collapse load of elastic elliptic torus.

Figure 19 shows curves of collapse load vs. a/b. When $a/b = 1$, the elliptic torus becomes a circular torus with radius $0.3m$. Figure 19 shows that the collapse load increases gradually with as a/b increases. When $a/b = 1$, the maximum load point appears at a displacement of $0.1m$, occurring earlier compared to other models. When b is close to a, it has a significant influence on the buckling of a half-elliptic torus. When interlaced displacement appears between the inner and outer equators, the stiffness generated by the minor axis b must first be overcome. In this case, local buckling occurs, and as the displacement increases, it turns into global buckling. If b is less than a, its influence can be omitted, and

Preprints (www.preprints.org) | NOT PEER-REVIEWED | Posted: 27 January 2022 doi:10.20944/preprints202201.0409.v1

only global buckling appears.

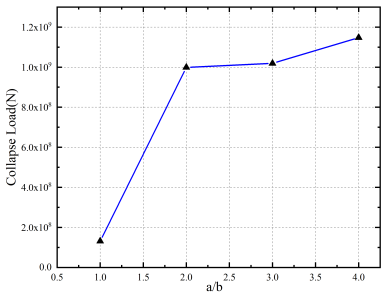

Figure 19: Collapse load vs a/b curves, $a/b = 1, 2, 3, 4$. When $a/b = 1$, the elliptic torus become a circular torus with $a = 0.3m$. Parameters a and b are major and minor axes, respectively.

V. CONCLUSION

We studied the nonlinear Gol'denveizer problem of circular and elliptic tori using the finite element method. It was demonstrated that finite element predictions are in good agreement with the results based on the membrane theory of Audoly and Pomeau [15] and bending theory of Sun [17]. We researched the mechanical properties of half-elliptic tori and half-toroidal shells in the nonlinear Gol'denveizer problem using FEM, and we showed the displacement, bending moment, membrane force, and shear force nephograms. We investigated the buckling mechanical properties of the Gol'denveizer problem of half-circular tori, and we showed the buckling failure mode. As a increased, half-circular tori had more rich buckling phenomena. We performed a nonlinear buckling analysis of half-elliptic tori, and we found a buckling phenomenon that we call a "skirt" shape. The collapse load of a half-elliptic torus of the Gol'denveizer problem increased gradually with a/b.

[1] Clark R A. On the theory of thin elastic toroidal shells[J]. Journal of Mathematics and Physics, 1950, 29(1-4): 146-178.
[2] Novozhilov. V. V. The theory of thin shells, Noordhoff, Groningen, (1959).
[3] SANDERS JR J L, LIEPINS A A. Toroidal membrane under internal pressure[J]. AIAA Journal, 1963, 1(9): 2105-2110.
[4] Libai A , Simmonds J G , Sanders J L . The Nonlinear Theory of Elastic Shells[M]. Academic Press, 1989.
[5] Zhang R J. Toroidal shells under nonsymmetric loading[J]. International journal of solids and structures, 1994, 31(19): 2735-2750.
[6] Reddy J N . Theory and Analysis of Elastic Plates and Shells[M]. 2006.
[7] Sun, Bohua. Closed form Solution of Axisymmetric Slender Elastic Toroidal Shells[J]. Journal of Engineering Mechanics, 2010, 136(10):1281-1288.
[8] Wang X H , D Redekop. Natural Frequencies Analysis of Moderately-Thick and Thick Toroidal Shells[J]. Procedia Engineering, 2011, 14(2259):636-640.
[9] Sun B . Toroidal Shells[M]. 2012.
[10] Sun B . Small symmetrical deformation of thin torus with circular cross-section[J]. Thin-Walled Structures, 163.
[11] Sun B . Nonlinear Elastic Deformation of Mindlin Torus. 2021.
[12] Goldenveizer A L , Herrmann G , Naghdi P M . Theory of Elastic Thin Shells[J]. Journal of Applied Mechanics, 1963, 30(3):479.
[13] W Flügge. Stresses in Shells[D]. Springer Berlin Heidelberg, 1973.
[14] B.H.Sun, Geometry-induced rigidity in elastic torus from circular to oblique elliptic cross-section, International Journal of Non-Linear Mechanics 135 (2021) 103754.
[15] Audoly, Y. Pomeau, The elastic torus: anomalous stiffness of shells with mixed type[J]. Comptes Rendus Mécanique, 2002, 330(6):425-432.
[16] Audoly, Y. Pomeau, Elasticity and geometry: from hair curls to the non-linear response of shells, Oxford university press, 2010.
[17] Sun B H. Gol'denveizer's problem of elastic torus[J]. Thin-Walled Structures, 2022, 171: 108718.